Space-oriented adiabatic demagnetization refrigerator adapted for quantum applications

A Léon[1], A Attard[1], J-L Durand[1], C Marin[2], S Martin[1] and J-L Duval[1*]

[1] Université Grenoble Alpes, CEA, IRIG-DSBT, 38000 Grenoble, France
[2] Université Grenoble Alpes, CEA, IRIG-PHELIQS, 38000 Grenoble, France

[*]E-mail: jean-marc.duval@cea.fr

Abstract. Adiabatic demagnetization refrigeration (ADR) is a candidate for being an alternative to helium-based dilution refrigeration for low power, low temperature applications. In particular, the CRYONEXT program aims to build ADR stages for the 20 mK – 3 K temperature range, the coldest stage providing up to 1 µW at 20 mK for quantum applications. We report here on the development process of such a stage. The setup is based on the space environment expertise of the laboratory which is transferred to build a prototype for cooling ground quantum applications. The focus is on a numerical tool created to optimize ADR stages dimensions, namely those of the paramagnetic material, superconducting coil, magnetic shield, and heat switch, and to predict the efficiency of the overall ADR device. The code is based on thermodynamic equations and a strong experimental database (magnetic properties of materials, ultra-low temperature magnetic hysteresis curves, thermal conductances, and heat losses). The performances estimated by the code were compared to those measured on a 1.8 K – 4.5 K ADR prototype. A relative difference lower than 10% in the released energy allowed the validation of the code and emphasized the critical importance of the magnetocaloric material conductivity and thermal contact resistance. For the present project, the code predicts a 2.7 kg 20 mK ADR stage which would provide 1 µW for 8 h. In addition to the dimensions of the magnetocaloric materials and their coils, the code provides insights on the critical parts of the design, which should be addressed to guarantee the success of the project. Here, the main heat loss is highlighted to be caused by the OFF conduction of the heat switch.

1. Introduction

Quantum devices require cryogenic temperatures ranging from 80 K for quantum communication [1], to 2-4 K for optical quantum devices like superconducting nanowire single photon detectors [2, 3] to subkelvin temperatures for quantum sensors and quantum materials characterizations [4, 5]. The national French program CRYONEXT is divided into seven projects which aim to develop the associated enabling cryogenic technologies. Among them, adiabatic demagnetization refrigeration (ADR) is especially identified as a complementary technology to dilution refrigeration [6, 7] for cooling below 100 mK. Indeed, despite producing less cold power, its lower complexity can fulfill the cooling needs of embedded sensors. Laboratory characterization experiments for quantum materials are also identified as possible applications.

In this context, multi-ADR stages will be designed to supply 1 µW at 20 mK for 8 hours and 200 µW at 400 mK continuously. We report here on the design process of the single shot 20 mK ADR stage. For that purpose, a numerical tool has been developed and experimentally validated on different temperature ranges. It concludes on the possible dimensions of the 20 mK stage and its efficiency with respect to Carnot efficiency, and it highlights room for improvement.

2. Numerical approach

2.1 Description of the system

An ADR stage is composed of four main elements: an ADR core, a superconducting coil, a ferromagnetic shield and a heat switch (HS). An ADR core refers to the magnetocaloric material and its copper thermal bus. Cooled sensors used in telescopes for space missions or embeddable quantum radars require ADR-based cryocoolers that must be light and compact. A code has been developed in Python and aims at minimizing the mass of the couple {ADR core, superconducting coil} for each ADR stage. Both an ADR pair - providing constant temperature thanks to a continuous ADR (cADR) and a single shot ADR (sADR) put in series - and a simple sADR can be designed. The numerical approach explained here focuses on the design of an ADR pair. The calculation is quasi-stationary since two main stationary phases were highlighted. The phases are named with respect to the sADR of the pair: the cold phase - sADR is cold and thermally connected to cADR that is being magnetized; and the magnetization phase – sADR is being magnetized thanks to the superconducting coil. Transition phases are neglected. Heat is extracted through the warm interface, seen in Figure 1(a) and (b). Total duration of a magnetic cycle is written as Δt_{cycle}.

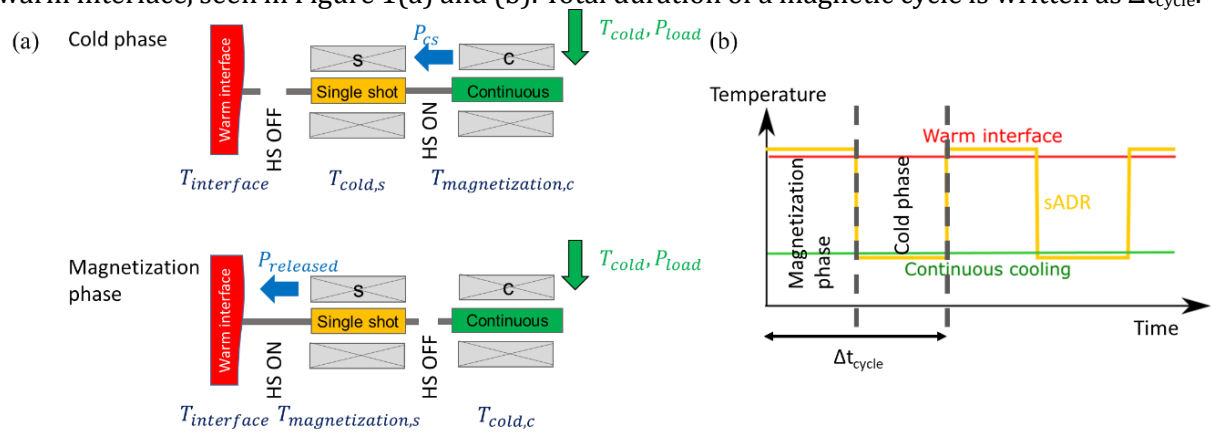

Figure 1. (a) Scheme of an ADR pair composed of a cADR (green) and a sADR (yellow). T_{cold} stands for the cold temperature of the cADR copper cold end, $T_{interface}$, also called T_{hot}, refers to the warm interface temperature. P_{load} is the expected cold power, P_{cs} and $P_{released}$ are the heat extracted through the heat switches when respectively the cADR and the single shot ADR are being magnetized. (b) Evolution of the temperature of the cADR, sADR and warm interface over time.

2.2. Description of the numerical approach

The calculation is divided into four steps:

1) Evaluation of the heat losses;
2) Power balance over the whole system;
3) Calculation of the thermal conductances, the powers, and the temperatures at each location of the ADR pair and for the two phases;
4) Minimization of the ADR core and superconducting coil masses;
5) Calculation of the efficiency of the pair with respect to the Carnot efficiency.

1) Heat losses originate from several sources and during several cycle durations. First, radiations arise onto the ADR cores from the coil mandrel, which are kept at the same temperature as the warm interface. Then, conduction arises through the Kevlar suspensions which support the cores in the middle of their shield and through the HS. A gas gap HS is the technology we chose for ADR stages. It is ON when the gap between two copper pieces is filled with helium, which ensures conduction. When the gap is empty, the HS is OFF. An adsorption pump made of charcoal and a heater ensures the ON/OFF transitions. During the cold phase, the s/interface HS is responsible for heat loads due to conduction through its stainless-steel outer envelope (a1). The s/c HS is ON (pump is heated) and conduction arises through the capillary, by the capillary wall and the gas inside (b). During the magnetization phase, the c/s HS is also responsible for heat loads due to conduction through its stainless-steel outer envelope (a2). Finally, there is also conduction through the capillary of the c/s HS as the capillary is thermally connected to the hot sADR (c). The total energy corresponding to the losses is written as E_{losses}. An example is given in Figure 4(a).

2) For both the cold phase and the magnetization phase, a power balance is done on the copper cold ends of each ADR core.

3/4) According to the second law of thermodynamics applied to an ideal ADR cycle that goes from 0 T to B_{max} and from T_{hot} to T_{cold}, the available energy E_{avail} of an ADR core which mass is m_{core} is equal to:

$$\boldsymbol{E_{avail} = \Delta S_{avail}(T_{cold}, T_{hot}, B_{max}) \times T_{cold} \times m_{core}} \quad (1)$$

where $\Delta S_{avail} = S(0, T_{cold}) - S(B_{max}, T_{hot})$ with S being the core magnetic massic entropy. The latter is computed according to the free ion model. An example is given in Figure 2(a) for Ytterbium Gallium Garnet $Yb_3Ga_5O_{12}$ (YbGG) [8]. When a significant difference occurs between our in-house experimental measurements and calculations, a correction factor is applied. This is especially the case for frustrated materials which deviate from the above-mentioned ideal model. For the cADR, the available energy must compensate for the addition of the load P_{load} and the heat losses that occur when the cADR is cold, so that $E_{avail}/\Delta t_{cycle} = P_{load} + P_{losses}$. The released energy from cADR to sADR is $E_{cs} = E_{avail} \times T_{hot} / T_{cold}$ [9] and can be expressed in terms of power P_{cs} with respect to the cold duration (cADR is magnetized when sADR is cold). The hot and cold temperatures refer to the magnetocaloric material's temperatures and are different from the copper cold end temperatures because of conduction within the material and thermal coupling between the material and the copper bus, see in Figure 2(b).

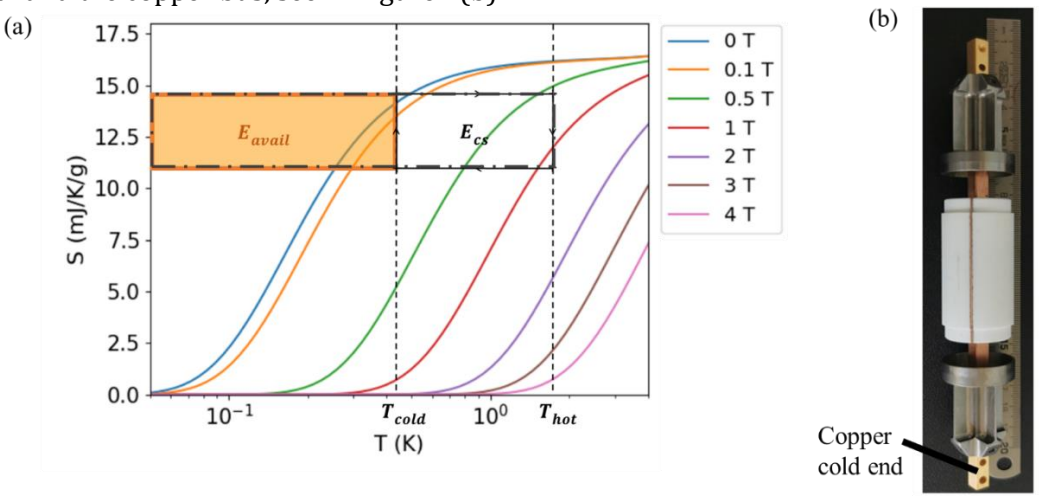

Figure 2. (a) Thermal dependence of the massic entropy of an YbGG core derived from the free ion model. An ADR cycle is represented between T_{hot} and T_{cold}. The orange area is proportional to E_{avail}, and the rectangular dotted area is proportional to the released energy E_{cs}. (b) YbGG core composed of the material and a copper bus.

For the sADR, the method is the same, but the load becomes P_{cs}. The thermal contact resistances between the ADR copper cold end and the c/s HS on one end and the thermal resistance of the HS itself on the other end should be taken into account. They were measured, and experimental fits are entered into the code.

5) Since the thermal links are not ideal and since several heat losses occur on the ADR pair, the efficiency of the thermodynamic cycle deviates from the Carnot efficiency. Contributions to this deviation are computed. The Carnot efficiency of 100 % corresponds to the ideal case of a released heat $E_{released}$ equal to the load energy of the cADR, $E_{load} = P_{load} \times \Delta t_{cycle}$ multiplied by the ratio of interface temperatures. Ideally the cADR runs from T_{cold} to T_{cold} if there is no thermal gradient in the ADR core whereas the sADR run from T_{cold} and $T_{interface}$, so that:

$$E_{transferred}^{Carnot} = E_{cs} \times \frac{T_{interface}}{T_{cold}} = E_{load} \times \frac{T_{cold}}{T_{cold}} \times \frac{T_{interface}}{T_{cold}} \quad (2)$$

The real $E_{released}$ when considering the heat losses and the thermal links is expressed as:

$$E_{transferred} = (E_{load} + E_{losses}) \times \frac{T_{c,hot}}{T_{c,cold}} \times \frac{T_{s,hot}}{T_{s,cold}} \quad (3)$$

where $T_{c,hot}$, $T_{c,cold}$, $T_{s,hot}$ and $T_{s,cold}$ are respectively the hot and cold temperatures of the cADR core and sADR core. The efficiency of the stage is defined as $E_{transferred}/E_{transferred}^{Carnot}$. In the next section, an experimental validation of the code is run on an ADR pair.

3. Experimental study

3.1. Experimental setup

An experimental demonstrator, originally built for the LiteBIRD mission, was used to run an ADR cycle with the following characteristics: the warm interface is maintained at 4.5 K and the cADR provides a continuous cooling of 1.23 mW at 1.8 K for 14 minutes. The total duration of the cycle is $\Delta t_{cycle} = 39$ min. Characteristics of the stages are listed in Figure 3(a) and a picture of the demonstrator is shown in Figure 3(c). Figure 3(b) exhibits the measured time evolution of the temperatures of the ADR pair copper cold ends.

(a)

	Demonstrator
cADR	YbGG, 52 cm³ – 1.5 T
sADR	YbGG, 70 cm³ – 2.8 T
HS c/s and s/interface	Gas gap

(b)

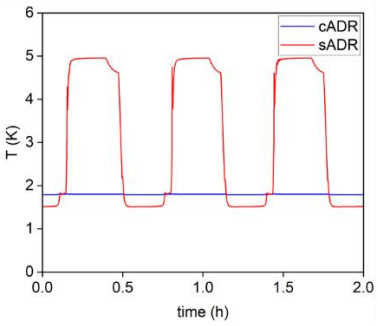

(c)

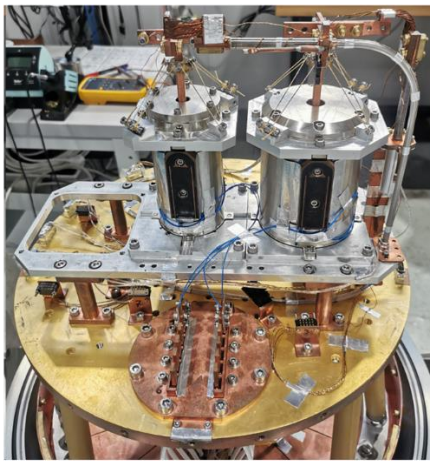

Figure 3. (a) Table of the ADR pair characteristics. (b) Time evolution of the copper cold end temperatures of the cADR and sADR. (c) Photograph of the ADR pair from the LiteBIRD demonstrator. The cADR iron shield can be seen on the left whereas the sADR is bigger, on the right.

3.2. Results

Computed heat losses are represented on the pie chart in Figure 4(a) in terms of power averaged over a whole ADR cycle. Because the losses impact different phases of the cycle, the associated losses in terms of power cannot be directly compared, unless they are averaged or converted in terms of energy. For convenience, only the averaged powers are presented here. The total heat losses averaged over the whole cycle are equal to 16.5 µW for the cADR and 28.8 µW for the sADR.

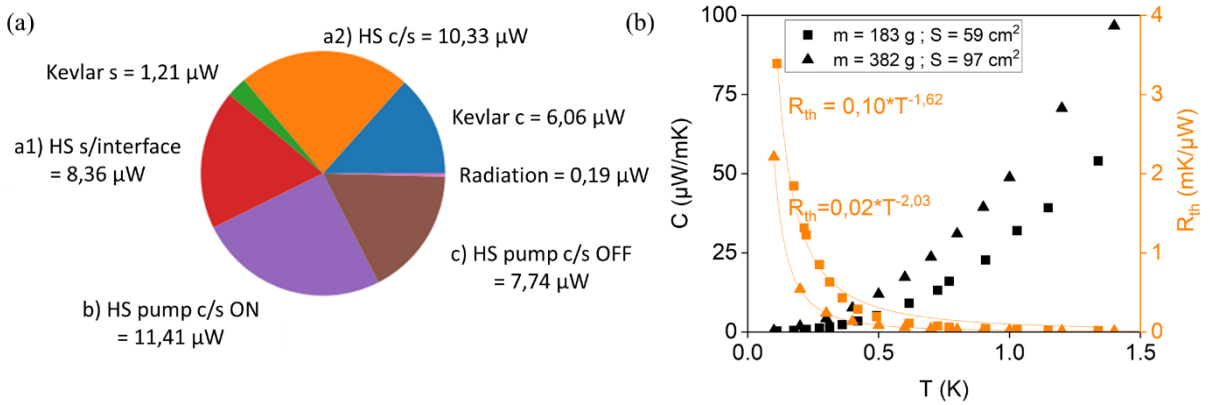

Figure 4. (a) Pie chart of the heat losses on the ADR pair. Losses a1), a2), b) and c) refer to the denomination from section 2.2. (b) Thermal evolution of the thermal conductance (black) and thermal resistance (orange) of two YbGG cores of different masses and contact surfaces S with copper. Associated fits show the almost T^2 dependence which is in agreement with a combination of metal-like conduction originating from the copper plates ($\propto T$) and an insulator-like behaviour ($\propto T^3$) associated to non-metallic part such as YbGG. The thermal conductivity of the latter was measured and published by Paixao Brasiliano D. A. et al. [8].

The measured sADR copper cold end temperatures equal 4.95 K and 1.52 K for, respectively, the magnetization phase and the cold phase. The heat rejected on the interface is measured as $P_{released}$ = 9.50 mW. The code is run with the following requirements: P_{load} = 1.23 mW, T_{cold} = 1.8 K, and $T_{interface}$ = 4.5 K. The estimated sADR copper cold end temperatures equal 4.76 K and 1.59 K for, respectively, the magnetization phase and the cold phase. The power released from the ADR pair to the interface is 8.00 mW. The relative difference between the measured and estimated released power, equal to 16 %, is satisfactory.

Since the powers and temperatures are computed from the cold part of the system to the interface, uncertainties occurring on the cold part can have tremendous effects on the sADR sizing and on the released energy. Such uncertainties mainly originate from the method used to assess the thermal resistances, based on fitting measurements. Firstly, the ADR core thermal resistance is measured assuming that the core is homogeneous and that the short-time measurements are comparable with long-time scale ones as described in [10]. The thermal conductance depends on the surface of the core in contact with the copper bus, hence on the core dimensions, which are to be optimized see in Figure 4(b). Secondly, thermal contact resistances can hardly be predicted since measurements are reproducible with uncertainties ranging from 2% to 20% [11]. For these reasons and to ensure a margin, the thermal contact resistances between the different components and thermal resistance within the ADR core are each multiplied by 1.3. The code is rerun with such a correction factor of 30%. The sADR copper cold end temperatures are consistent with the measured ones: 4.87 K and 1.53 K for, respectively, the magnetization phase and the cold phase and the relative difference between the released powers is less than 10 % since $P_{released}$ = 8.65 mW from the code.

Comparisons between the measured and the predicted released energy $E_{released}$ are further analysed when put in perspective with the energy released by a Carnot cycle. The bar chart Figure 5 shows the contributions of the heat losses, the sADR core thermal resistances and the thermal links (HS, strap and thermal contacts) resistances to the increase of the released energy and the decrease of the efficiency with respect to the Carnot efficiency. For the present stage, the heat losses only represent a relative loss in the Carnot efficiency of 4%. Yet, the thermal links (HS, copper strap and thermal contact resistance) between cADR and sADR decrease the efficiency by 15% versus experimental data.

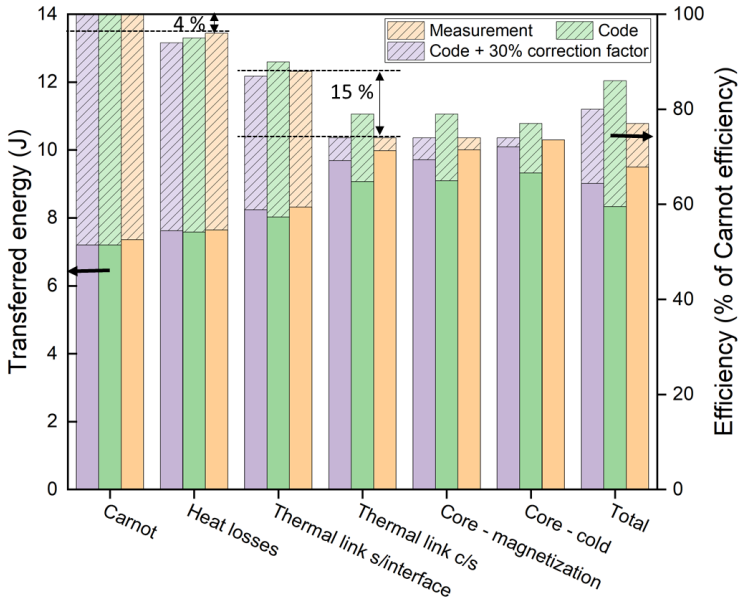

Figure 5. Bar chart of the efficiency of the ADR pair (hatched surface) and the associated energy released to the interface (plane surface). The graph highlights the contributions of the heat losses and the thermal link to those two performance parameters. The percentages indicated are the relative differences between the two consecutive efficiencies.

The calculation processed on the 1.8 K – 4.5 K ADR pair can be extended to the temperature range [10 mK; 5 K] when knowing the properties of the magnetocaloric materials and the thermal resistances of the thermal links.

4. Toward a 20 mK stage

A 5-stage ADR cooler design may be adopted for the CRYONEXT program, similar to the 50 mK multistage assembly chosen for the ATHENA space mission [12], which design is calculated using the above-mentioned method. A diagram of the three coldest stages considered is shown in Figure 6. For such development, the 20 mK sADR stage is the most critical so its design is addressed here.

The stage is sized to provide P_{load} = 1 µW at 20 mK for eight hours with an interface at 400 mK. The total duration of the magnetic cycle is 16h. A gas gap heat switch will be used and for this preliminary estimation, its dimensions are based on well-known sizing from previous projects. The magnetocaloric material chosen for the first phase of the project is Cerium Magnesium Nitrate, $Ce_2Mg_3(NO_3)_{12}$ $24H_2O$ (CMN). Our calculation is based on the magnetic properties of the materials derived from the free ion model.

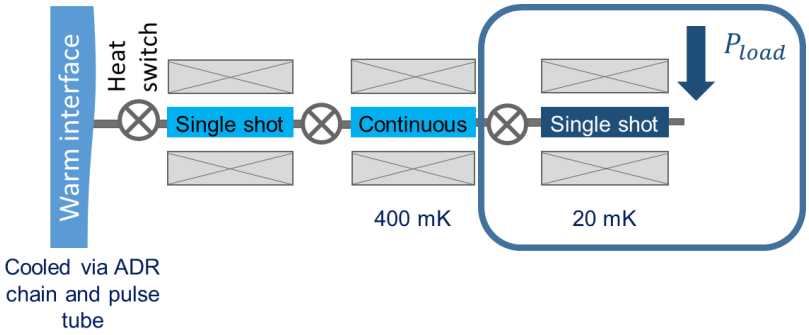

Figure 6. Diagram of the 3-ADR chain under design for the CRYONEXT program, composed of an ADR pair and a sADR. The sizes and the efficiency of the sADR stage circled in blue are predicted with the code.

The conductance of the CMN core, that is CMN material's conductance and coupling with the copper cold end, is critical for the operation and for the sizing of this ADR. Currently, no data are available. The common value of 80% was set for the efficiency of the stage, in order to compute orders of magnitude of the CMN core conductance. Values of 0.3 mK/µW at 400 mK and 2.6 mK/µW at 20 mK are taken. The gas gap HS originates an averaged conduction loss of 0.045 µW on the sADR stage (applied during the cold phase). For Kevlar suspensions, similar design as for space applications is chosen. Conduction through the latter results in 0.006 µW heat loss on the sADR copper cold end. The mechanical specifications for quantum applications will be easier to fulfil than for space applications and reduced Kevlar sections will lead to lower losses. Radiation losses have been neglected. The total averaged losses are equal to 0.051 µW.

With a correction factor of 30% on the thermal contact resistances, we used our calculation to minimize the total mass of the stage for a given cooling power. This led the sADR CMN core to have a volume of 183 cm^3 at an optimum magnetic field of 0.87 T. Of note, the latter is well below the saturation magnetic field of CMN, which is 2 T [13]. The addition of the optimized mass of the pair {ADR core, superconducting coil} and a predicted non-fully-optimized magnetic shield equals 2.7 kg. Because of the thermal links within the ADR core, maintaining the sADR copper cold end at 20 mK requires the CMN core cold temperature to be 18 mK. The core temperature during magnetization is equal to 425 mK. Released power to the 400 mK cADR stage equals 27 µW. This heat load can be absorbed by the 400 mK stage. The total efficiency of the stage is computed using the method from part 2.2. Total heat losses represent 9% lost on the efficiency and 6% are lost due to the 20 mK thermal resistance of the CMN core. Conductance measurements are planned on real samples to better assess this value, depending mostly on the CMN coupling with the copper cold end [13] and if necessary, specific design will be put in place. Reducing conduction through the HS and the Kevlar suspensions and increasing the CMN core thermal conductance constitute room for improvement.

A critical aspect for 20 mK operation is accurate temperature measurements, especially when high temperature stability is required. As part as other projects, we developed 50 mK temperature read-out system dedicated to space instrument development. To extend these capabilities down to 20 mK, it is necessary to decrease the excitation level of the sensor from 2 nA to about 10 pA to avoid self-heating. Cold filtering becomes important and will be studied to minimize EMC disturbances. This development will be integrated into the FlexCryo instrumentation developed by CEA/DSBT [14].

5. Conclusion and perspectives

A numeric tool for optimizing the dimensions of sADR stages and ADR pairs has been developed. The computed temperatures and the released energy to the interface are compared to measurements done on a 1.8 K – 4.5 K ADR pair prototype. The estimated released power is in good agreement with the measured one since the relative difference between the two values equals 10%. Such a difference can be partially explained by the uncertainty in the measured thermal conductances of the ADR cores and in the thermal links resistances (HS, strap and thermal contacts). Comparisons between the efficiencies of the theoretical and experimental pairs with respect to the Carnot efficiency on one hand and predicted and measured temperatures on the other end reveal that a correction factor of 30% is needed to better mimic the behaviour of the prototype.

The code is used with this correction factor to predict the sizing of the 20 mK sADR stage that will be built for CRYONEXT program. Such a stage should provide 1 µW at 20 mK for 8 hours. With a total mass of 2.7 kg, the sADR stage should release 27 µW to the 400 mK cADR stage. Further optimization of the magnetic shield dimensions could lower the total mass of the stage. The thermal conductance values of the CMN core should be confirmed by future measurements. This should lead to a more precise estimation of the efficiency of the stage. Further gains could be obtained with efforts on the thermal links design and by reducing the conduction losses.

Acknowledgments

We thank ANR for supporting this development as part of CRYONEXT and ASIS program.

References

[1] Luo W, Cao L, Shi Y, Wan L, Zhang H, Li S, Chen G, Li Y, Li S, Wang Y, Sun S, Faeyz M K, Cai H, Kwek L C and Liu A Q 2023 *Light Sci. Appl.* **12** 175.
[2] Dang H, Zhang T, Zha R, Tan J, Li J, Zhao Y, Zhao B, Tan H and Xue R 2019 *IEEE Trans. Appl. Supercond.* **29** 5.
[3] Steinhauer S, Gyger S and Zwiller V 2021 *Appl. Phys. Lett.* **118** 100501.
[4] Yamashita T, Miki S, Qiu W, Fujiwara M, Sasaki M and Wang Z 2011 *IEEE Trans. Appl. Supercond.* **21** 336-339.
[5] Hazra D, Kirtley J R and Hasselbach K 2013 *Appl. Phys. Lett.* **103** 093109.
[6] Mazin B A, Meeker S R, Strader M J, Skypryt P, Marsden D, van Eyken J C, Duggan G E, Ulbricht G and Johnson M 2013 *PASP* **125** 1348.
[7] Shirron P J 2014 *Cryogenics* **62** 130-139.
[8] Paixao Brasiliano D A, Duval J-M, Marin C, Bichaud E, Brison J-P, Zhitomirsky M and Luchier N 2020 *Cryogenics* **105** 103002.
[9] Pobell F 2007 Springer.
[10] Luchier N, Duval J-M, Duband L and Tirolien T 2012 *Cryogenics* **52** 4–6: 52-57.
[11] Xian Y, Zhang P, Zhai S, Yuan P and Yang D 2018 *Appl. Therm. Eng.* **130** 1530-1548.
[12] Duval J-M, Bancel F, Charles I, Durand J-L, Léon A, Lizion J, Marin C, Martin S and Prouvé T 2024 *Cryocoolers* **23** 323-331.
[13] Bromiley P A 1999 Thesis.
[14] Attard A, Bonnay P, Duband L, Duval J-M, Durand J-L and Jourdan T 2019 *CECICMC* hal-04779932.